Chapter 2
The LHCb Experiment at the LHC

The purpose of this chapter is to give a brief introduction to the LHCb detector, the experimental apparatus used to perform the analysis described in this thesis. The chapter starts with a description of the Large Hadron Collider (LHC) at CERN in Sect. 2.1, while the detector is described in Sect. 2.2. After an overview of the running conditions of the experiment in 2011 (Sect. 2.2.1), all subdetectors are described individually in Sect. 2.2.2 to Sect. 2.2.7. The trigger system is described in Sect. 2.2.8, focusing the attention on the hadronic lines used in the analysis (for a detailed description of trigger requirements, see Sect. 3.6). The chapter is then concluded by a description of the track reconstruction in Sect. 2.2.9, the definition of the combined particle identification (PID) likelihood variables in Sect. 2.2.10 and an overview of the LHCb software framework used in the analysis in Sect. 2.2.11.

2.1 The LHC at CERN

The LHCb detector is one of the main experiments at the Large Hadron Collider (LHC) [1]. The LHC is a *proton-proton* collider located at CERN (Conseil Européen pour la Recherche Nucléaire), situated on the Franco-Swiss border near the city of Geneva. With its design energy of $\sqrt{s}$ =14 TeV and a design luminosity of $10^{34}\text{cm}^{-2}\text{s}^{-1}$, it is the largest and the most powerful particle collider ever built. Approved in December 1994 and constructed from 1998 to 2008, this superconductive synchrotron is situated in the same 26.7 km tunnel used for the e^+e^- collider LEP, decommissioned in 2000 after more than 10 years of successful running. A schematic view of the LHC is presented in Figs. 2.1 and 2.2. The accelerator is divided in eight octants and beams circulate in opposite directions into two separate rings. Two separate rings, with opposite magnetic field, are required as the colliding particles carry the same charge. This has direct consequences on the design of the magnets, shown in Fig. 2.3, which excludes a common vacuum beampipe for both circulating rings. All superconductive magnets are cooled down to a

P. Gandini, *Observation of CP Violation in $B^{\pm} \to DK^{\pm}$ Decays*,
Springer Theses, DOI: 10.1007/978-3-319-01029-8_2,

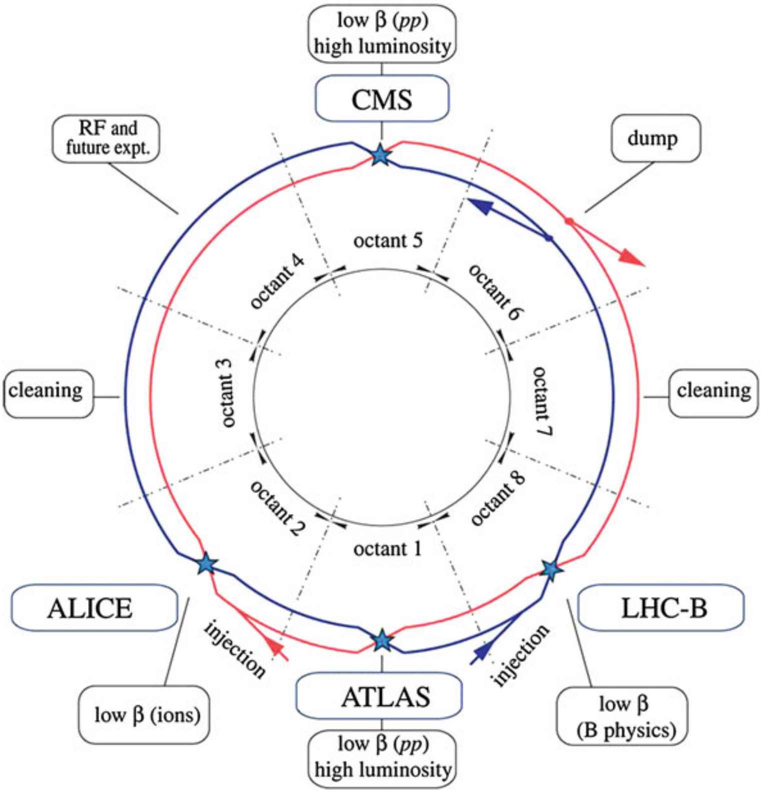

Fig. 2.1 A schematic layout of the LHC. Beam 1 runs clockwise, beam 2 anticlockwise

temperature of 1.9 K, using superfluid helium, to operate them safely at magnetic fields up to 8.3 T, depending on the energy of the beams. Protons are injected from the Super Proton Synchrotron (SPS) at the energy of 450 GeV and then accelerated to 3.5 TeV, providing collision at the total energy $\sqrt{s} = 7$ TeV. This corresponds to half of the design energy, which will be reached after upgrading the machine in 2013. Beams are kept separate in the machine and they only cross in four interaction points (IP), where the main experimental detectors are situated: ATLAS [2] and CMS [3] are hosted in IP1 and IP5 respectively, LHCb [4] in IP8 and ALICE [5] in IP2. The general purpose detectors ATLAS and CMS are designed to run at the highest possible peak luminosity of $10^{34}\,\text{cm}^{-2}\text{s}^{-1}$, while LHCb is designed to operate at a reduced instantaneous luminosity of $10^{32}\,\text{cm}^{-2}\text{s}^{-1}$ (for a detailed description of the running conditions of the LHCb detector, see Sect. 2.2.1). The high luminosity of the LHC is delivered through intense bunches consisting of 1.1×10^{11} protons each, separated by 50 ns intervals between each crossing (the design value is 25 ns corresponding to a frequency of 40 MHz).

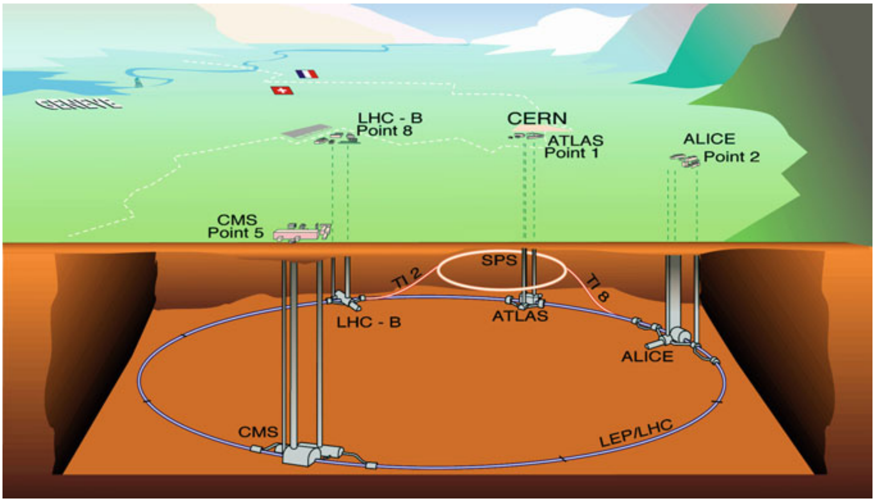

Fig. 2.2 A pictorial view of the LHC collider with its four interaction points The underground tunnel lies between 50 and 175 m below the surface on a plane inclined down about 1.4 % towards Lac Léman

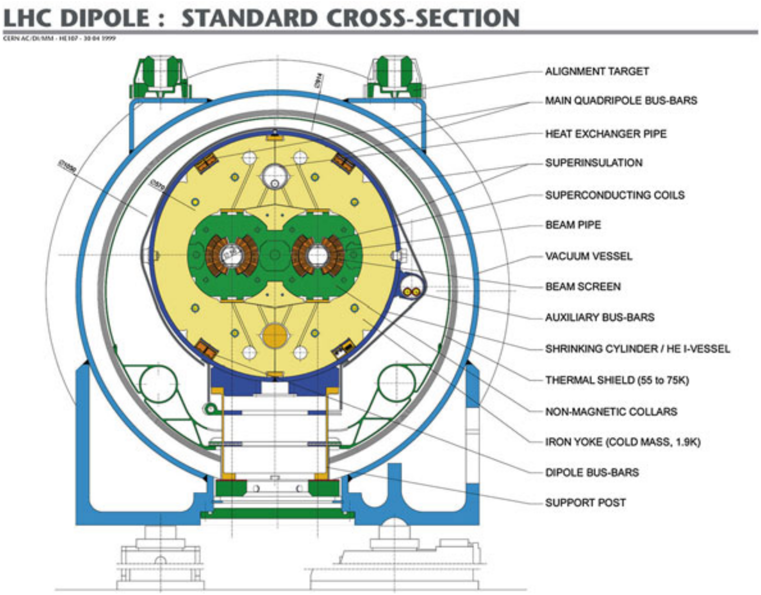

Fig. 2.3 Section of a LHC dipole magnet. The two separate rings are clearly visible and they are enclosed in the same cryostat

2.2 The LHCb Detector

The LHCb experiment is focused on the study of beauty and charm flavour physics at the LHC. With the large, measured $b\bar{b}$ production cross-section of $284 \pm 20 \pm 49$ mb [6] at $\sqrt{s} = 7$ TeV, it is the most abundant source of b-hadrons, which can hadronise into different species of B mesons, e.g B_d, B_u, B_s and B_c and other long lived Λ_b baryons. These unique properties allow studies of CP-violating phenomena, in both $B_{u,d}$ and B_s sectors, and rare decays with unprecedented precision. However, hadronic collisions result in a high-background environment, with events containing up to 300 charged tracks. The high luminosity delivered by the LHC also increases the chances of multiple interactions per event, making the reconstruction of b-hadron secondary vertices experimentally challenging.

The physics requirements needed for precise flavour physics studies, along with the experimental conditions, set stringent constraints on the performance of the LHCb detector. The key points can be summarized as follows:

- **Impact parameter and vertex resolution**
  An excellent vertex resolution is crucial in order to resolve secondary vertices coming from b-hadron and c-hadron decays with respect to the primary pp interactions. A performing proper time determination is particularly important for oscillation measurements, in particular for the fast oscillating B_s^0–$\bar{B}_s^0$ system. Furthermore, a good resolution provides a better distinction between displaced secondary tracks and prompt background tracks originating directly from the primary vertex. In the LHCb detector, vertexing is performed by the VErtex LOcator (VELO) subdetector, presented in Sect. 2.2.2, which is situated as close as possible to the interaction region.
- **Momentum and invariant mass resolution**
  A good resolution on the invariant mass of the reconstructed particles is needed to distinguish b-hadrons from random combinations of background tracks. Combinatorial background is expected to be a considerable source of background for physics analyses with hadronic final states.
- **Particle identification**
  Particle identification is an essential tool for any flavour physics experiment. Electrons and photons are identified via the electromagnetic calorimeter and muons are the only particles which can pass through the calorimeters leaving hits in the muon stations. As hadrons are difficult to distinguish using only information from the calorimeters, additional discrimination is needed to ensure a satisfactory pion, kaon and proton separation over a momentum range up to 100 GeV. Discrimination between charged hadrons is provided in LHCb by a Ring Imaging CHerenkov (RICH) system (Sect. 2.2.5), which uses three radiators with different optical properties.

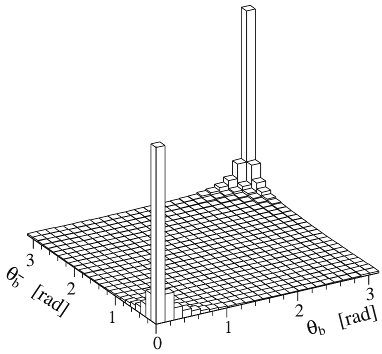

Fig. 2.4 Angular correlation between the b and $\bar{b}$ quarks produced in pp interactions (angles formed with respect to the beam axis). Events are simulated with the PYTHIA event generator [7]

- **Trigger**
  In a hadronic environment, b-hadron events are overwhelmed by uninteresting background events. A trigger system is required to select only useful collisions and reduce the total data bandwidth to an acceptable rate. The LHCb detector runs a multi-stage trigger, both hardware and software, which reduces the rate of visible interactions from about 10 MHz to about 3 kHz (Sect. 2.2.8). The system must be efficient and extremely flexible at the same time: it must select as many B final states as possible and adapt quickly to the variable LHC running conditions.

At the LHC, $b\bar{b}$ pairs are produced through the strong interaction and they carry the momentum of the partons involved in the hard collision. As the pp collision energy is much higher than the $b\bar{b}$ invariant mass, it is likely that there is considerable difference in the colliding partons' momenta. The $b\bar{b}$ pairs are therefore boosted in the direction of the most energetic parton, predominately at low angles in the laboratory system with respect to the beampipe. The trajectories of the resulting b-hadrons are highly correlated and concentrated in the forward/backwards regions of the colliding protons, as shown in Fig. 2.4. As a result of this forward production and the limited space available in the experimental area at IP8, the LHCb detector is designed as single-arm spectrometer with a coverage from approximately 10–300 (250) mrad in the horizontal bending (vertical non-bending) plane. This corresponds to a pseudorapidity[1] coverage of $1.9 < \eta < 4.9$. The LHCb detector is presented in Fig. 2.5. The interaction region is situated inside the VErtex Locator detector, at the left side of the plot, and it is displaced -11.25 m from the center of the cavern. The total length of the detector is about 20 m in the longitudinal direction (z-axis), 12 m in the horizontal direction (x-axis), and about 10 m in the vertical one (y-axis). The six subdetectors composing LHCb can be conveniently grouped as follows:

- **The tracking system** (Sects. 2.2.2, 2.2.3 and 2.2.4)
  composed by the VErtex LOcator (VELO), the LHCb magnet, the Tracker Turicensis (TT) and three tracking stations (T1,T2,T3).

[1] The pseudorapidity variable is defined as $\eta = -\ln\tan(\theta/2)$, with θ being the angle between the particle momentum and the beampipe.

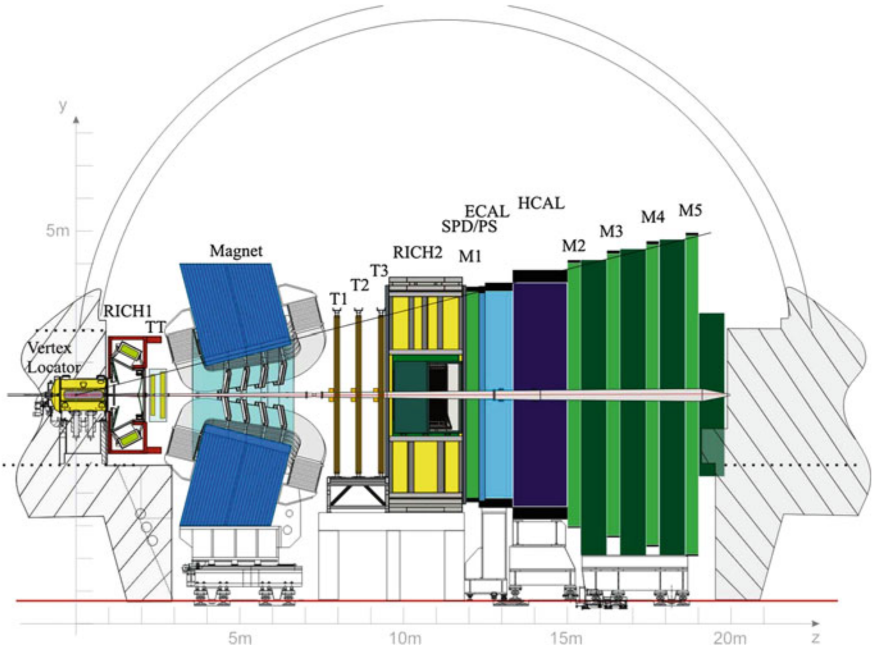

Fig. 2.5 Layout of LHCb detector on the transverse plane

- **The RICH detectors** (Sect. 2.2.5)
  composed by two separate systems RICH1 and RICH2.
- **The calorimeters** (Sect. 2.2.6)
  composed by the Scintillating Pad Detector (SPD), the Pre-Shower detector (PS), the Electromagnetic CALorimeter (ECAL) and the Hadronic CALorimeter (HCAL).
- **The muon stations** (Sect. 2.2.7)
  composed by five muon stations (M1,M2,M3,M4,M5).
- **The trigger system** (Sect. 2.2.8)
  composed by Level 0 (L0), High Level Trigger 1 (HLT1), High Level Trigger 2 (HLT2).

Each subsystem is described here briefly; detailed information on the LHCb detector can be found in its Technical Design Report [4].

2.2.1 LHCb Detector Running Conditions

This section presents a brief overview of the running conditions of the LHCb experiment in 2010 and 2011. The LHCb detector has performed well during both years, surpassing its target design luminosity and showing an excellent flexibility in adapting to the variable running conditions of the LHC. Two important parameters can be used to describe the operation of the LHCb detector: the instantaneous luminosity $\mathcal{L}$ and the average number of visible interactions per bunch crossing μ. In the LHCb interaction region, the luminosity is reduced and levelled in order to maintain a constant value during each fill. For the design luminosity $\mathcal{L} = 2 \times 10^{32}\text{cm}^{-2}\text{s}^{-1}$, the design μ is about 0.4–0.5, which means that the data collected with this experimental conditions should be dominated by events with one single primary vertex. In fact, a high value of μ indicates multiple pp interactions per event, resulting in high track multiplicity and increased background. The time needed to process every event by the trigger is also hugely affected as the number of track combinations scales factorially.

2010 Running Conditions

In 2010, the LHCb experiment collected about 37.7 pb^{-1}, with an average efficiency ($\mathcal{L}_{\text{recorded}}/\mathcal{L}_{\text{delivered}}$) of 89 %. Figure 2.6 shows the integrated luminosity recorded during 2010. Almost all data was collected in the last two weeks of running, reaching 80 % of the design instantaneous luminosity. However, the experimental conditions have been completely different from the design values, with an average value of $\mu > 2$ (see Fig. 2.7). As high values of μ greatly affected the event size and the online processing time, the trigger configurations and thresholds had to be changed regularly during 2010.

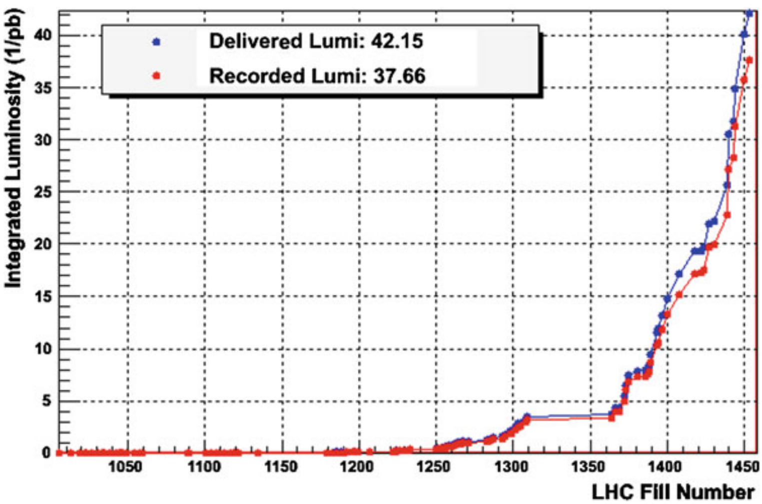

Fig. 2.6 Integrated luminosity versus LHC fill number delivered and collected in 2010

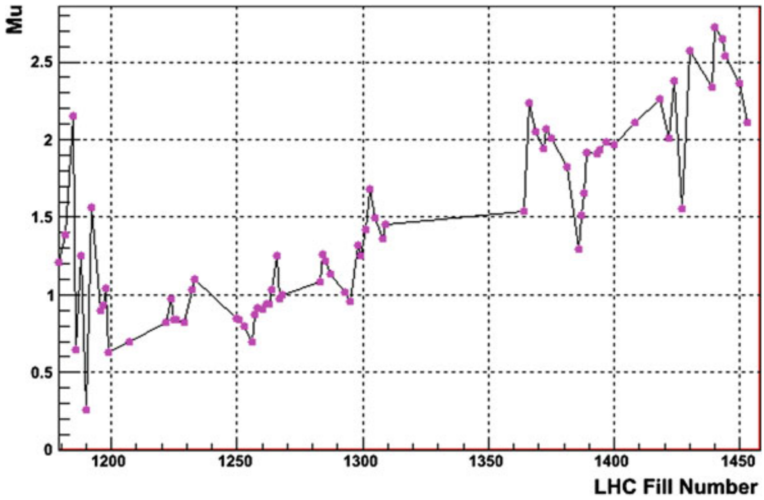

Fig. 2.7 Peak μ versus LHC fill number in 2010 (design value $\mu = 0.4$)

2011 Running Conditions

In 2011, data taking conditions were fairly stable at LHCb, recording more than 1 fb^{-1} of data at a constant pace, as shown in Fig. 2.8. The instantaneous luminosity was set to $\mathcal{L} = 3.5 \times 10^{32}$ $cm^{-2}s^{-1}$, without a significant loss of data quality. The measured μ during 2011 is shown in Fig. 2.9 and was about three times above its design value (but lower than what observed in 2010). These stable experimental conditions resulted in more homogeneous trigger setup, as shown in Table 2.1, with only five different Trigger Configuration Keys (see Sect. 2.2.8) contributing to more than 90 % of the total collected luminosity. This simplification helps with the systematic studies of the trigger acceptance.

2.2.2 VELO

The VErtex LOcator (VELO) [8] provides precise measurements of the track position in the region close to the pp collisions. Primary vertices are reconstructed using the prompt tracks coming directly from the pp interactions and, as most of the long-lived b and c-hadrons decay inside the VELO instrumented volume, displaced tracks are used to identify and reconstruct their secondary vertices with good accuracy. Displaced tracks are also used as a trigger criterion in the HLT1 (Sect. 2.2.8). The resolution on the primary vertex is found to be, on average, about 42 μm (10 μm) on the z coordinate (x–y transverse plane) and depends on the number of tracks in the event. In order to achieve the desired resolution, the detector is located as close as

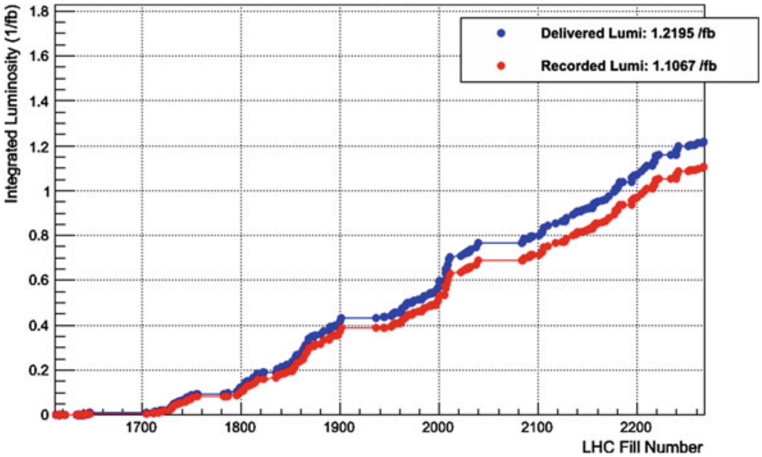

Fig. 2.8 Integrated luminosity versus LHC fill number delivered and collected in 2011

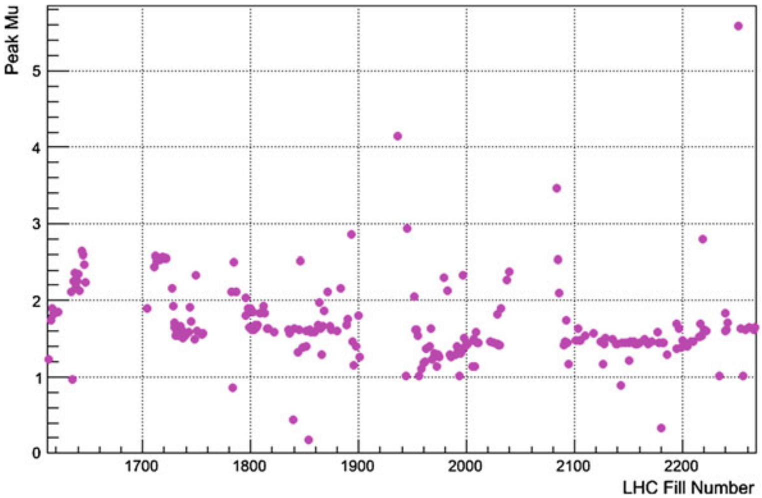

Fig. 2.9 Peak μ versus LHC fill number in 2011 (design value $\mu = 0.4$)

possible to the interaction region. The VELO layout is shown in Fig. 2.10: it consists of two sets of 21 modules positioned around the nominal interaction region perpendicularly to the beam axis. Each module provides an independent measurement of the r and ϕ cylindrical coordinates. The z coordinate is provided by the fixed z-position of the module itself.

Each station is formed by two semi-circular silicon detectors, with a sensitive region starting from 8.2 mm radially from the beam axis when the detector is operated in the *closed* position. The aperture increases during the LHC injection phase (*open* position) for safety reasons and the VELO is closed around the optimal beam

Table 2.1 List of TCKs used in 2011 data with the corresponding collected luminosities, split by magnet polarity

TCK	Magnet down	Magnet up	Total	(% rel.)
0x360032	3.36	-	3.36	(0.31)
0x480032	2.00	-	2.00	(0.18)
0x4A0033	2.09	-	2.09	(0.19)
0x561710	0.03	-	0.03	(0.00)
0x5A0032	28.45	38.63	67.08	(6.19)
0x5B0032	0.03	2.20	2.23	(0.21)
0x5D0033	-	2.25	2.25	(0.21)
0x6D0032	100.33	-	100.33	(9.25)
0x700034	1.14	-	1.14	(0.11)
0x710035	0.90	-	0.9	(0.08)
0x730035	61.83	134.35	196.18	(18.09)
0x740036		5.18	5.18	(0.48)
0x760037	191.64	107.11	298.75	(27.55)
0x790037	-	39.30	39.3	(3.62)
0x790038	209.43	153.97	363.4	(33.52)

Luminosities, expressed in pb^{-1}, are taken from the online LHCb $\mathcal{L}$ measurement. About 95 % of the integrated luminosity was collected with only five different TCKs

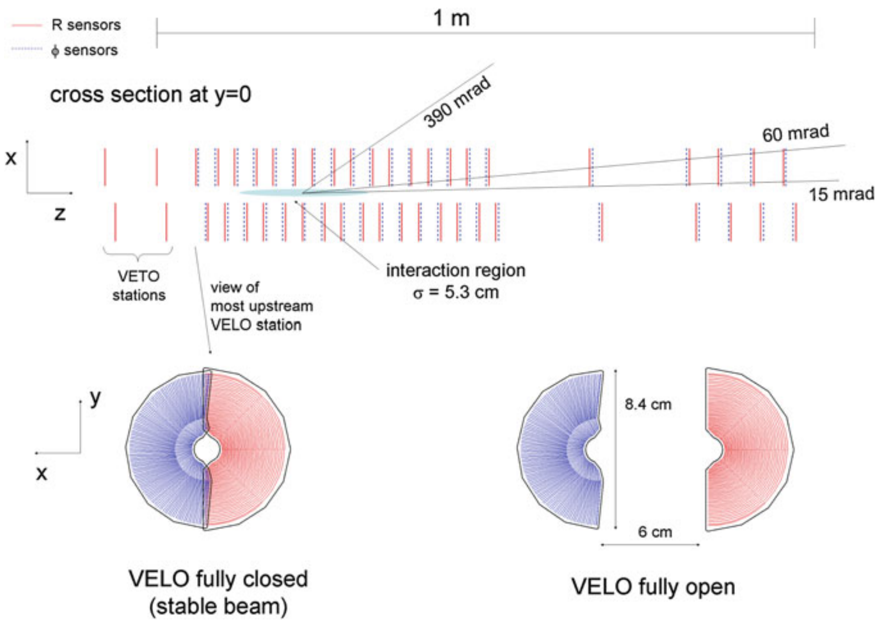

Fig. 2.10 *Top* layout in the x–z plane of the VELO sensors. The interaction region and angular acceptances are plotted. The acceptance region of the VELO is $1.6 < \eta < 4.9$. *Bottom* the front face of the first modules in the x–y transverse plane in closed (*left*) and open (*right*) position

x–y center only after stable beams are declared. For this purpose, the two halves of the detector are mounted on a controllable positioning system, located in a vessel that maintains the vacuum around the sensors, though separated from the machine vacuum by a thin walled corrugated aluminum sheet.

Two pile-up modules, containing only r-coordinate sensors, are located upstream of the VELO sensors. Those modules can be read at 40 MHz and they were originally designed to provide useful information to the L0 trigger (Sect. 2.2.8) in order to reject multiple interaction events. Given the changed experimental conditions (see Sect. 2.2.1), they are not currently used in the trigger.

2.2.3 Dipole Magnet

Charged tracks are bent in the horizontal plane with an intense magnetic field generated by a normal-conductive dipole magnet [9] weighting 1,600 tons. The LHCb magnet, shown in Fig. 2.11, provides an integrated magnetic field of 3.6 Tm. It is situated between the two RICH detectors and its magnetic field profile is designed in order to minimise the residual field inside the RICH1 boxes and the VELO, while creating a field as high as possible in the region before the tracking stations. In order to achieve the required momentum resolution, better than $\delta p/p \approx 0.5\,\%$ over a wide momentum range, the magnetic field must be known with a spacial precision up to a few millimeters.

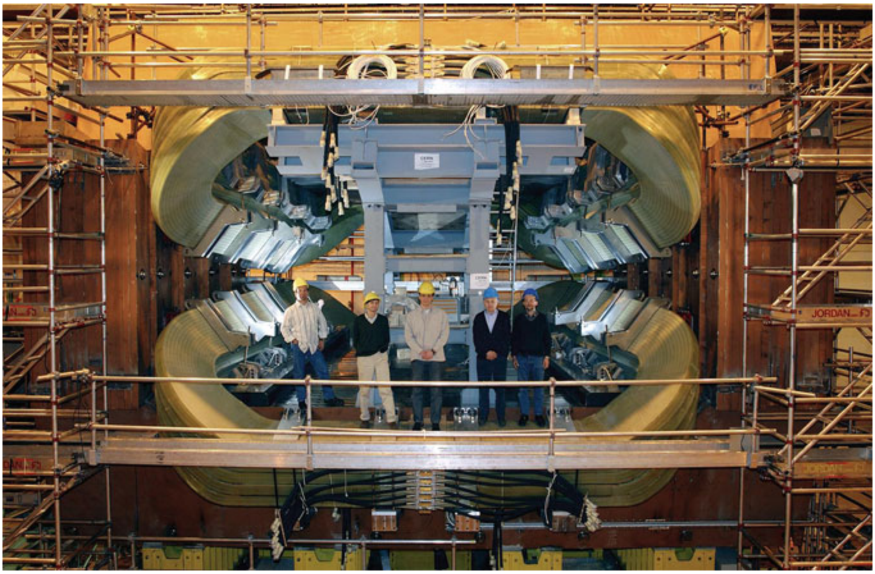

Fig. 2.11 View of the LHCb dipole magnet

2.2.4 Tracking Stations

The coordinates on the transverse plane of the charged tracks are measured by five planar tracking stations located at different z-positions. The first two layers (TT) are situated before the magnet, while the latter three (T1, T2, T3) after. T1, T2 and T3 are composed of two different types of detector, the Inner Tracker (IT) and Outer Tracker (OT), and they are optimised in order to maximise the momentum measurement resolution. The layout of the LHCb tracking system is shown in Fig. 2.12.

Tracker Turicensis (TT)

The Tracker Turicensis (TT) is a 130×150 cm ($8.4\,m^2$) planar tracking station and it is situated before the dipole magnet. It consists of four layers of silicon microstrips and covers the full LHCb acceptance. With a maximal strip occupancy of about 2.5 % in the region close to the beampipe, the expected spatial resolution is about 50 μm. These four instrumented layers are arranged in two pairs, separated about 27 cm in the

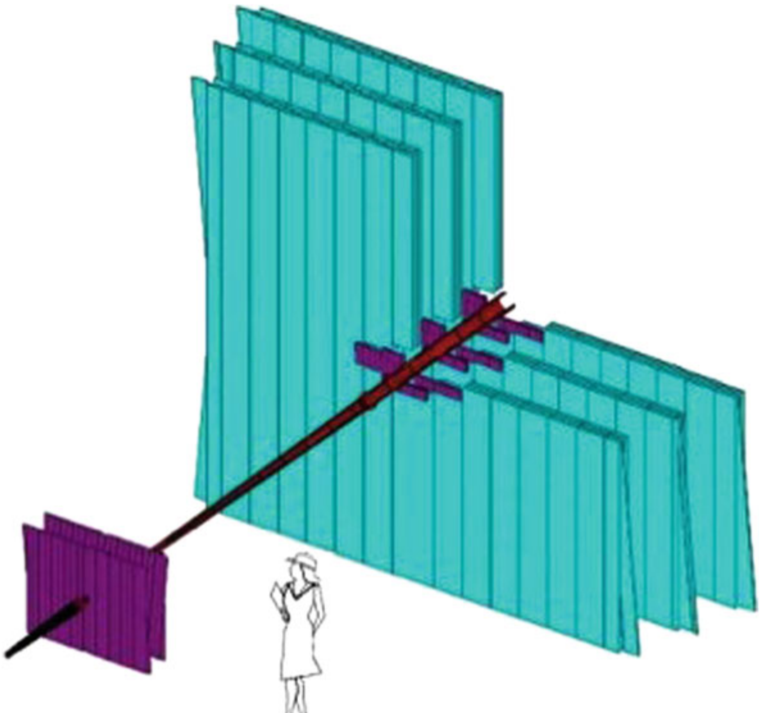

Fig. 2.12 Layout of the LHCb tracking system. The silicon microstrips of the TT and the IT are coloured in *purple*, the OT planes are shown in *blue*

z direction. The first and the last planes have vertical readout strips (x layer), while the second and the third have strips rotated by a small angle of $\pm5^\circ$ respectively (u and v layers). This small stereo angle is chosen to maximise the momentum resolution, as charged particles are mainly bent in the horizontal plane. Information coming from the TT detector is important for the reconstruction of long-lived neutral K_s^0 mesons, that decay mostly outside the fiducial volume of the VELO. With a $c\tau \approx 2.7$ cm and relativistic factors γ of 10–100 at the LHC, K_s^0 mesons can travel up to several meters before decaying.

Inner Trackers (IT)

The Inner Tracker (IT) [10] composes the central part of the tracking stations situated after the dipole magnet. It covers the acceptance region close to the beampipe, where the particle flux is highest, and uses the same silicon strip technology as the TT. The cross-shaped layout of the detector (120×40 cm) covers only 1.3 % of the total sensitive area of each tracking plane, with a spatial resolution of 57 μm. However, as most of the tracks are produced in the forward/backward region along the beamline, about 20 % of the total number of charged tracks in each event is concentrated in this region. The Inner Tracker is shown in Fig. 2.13.

Outer Trackers (OT)

The Outer Tracker (OT) [11] is a drift-time detector providing acceptance coverage in the outer region of the tracking stations. Each module is composed of four layers of drift-tubes with diameters of 4.9 mm. The geometry of the four layers is identical to that of the TT detector, with the second and third layers rotated by a $\pm5^\circ$ stereo

Fig. 2.13 A view of the IT

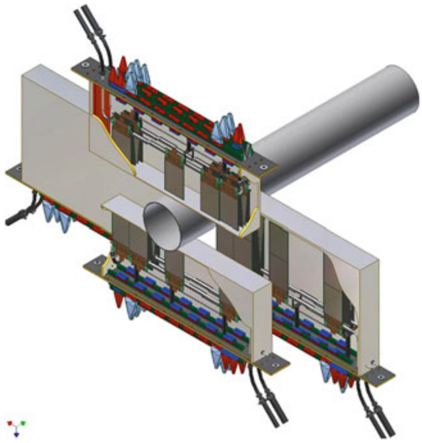

Fig. 2.14 A view of the OT

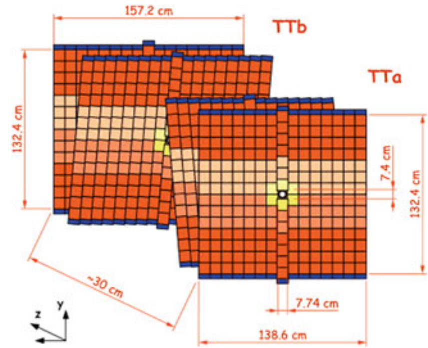

angle. Each drift-tube is filled with a mixture of Argon (70 %) and CO_2 (30 %), with drift times below 50 ns. The layout of the Outer Tracker is shown in Fig. 2.14.

2.2.5 RICH

Discrimination between charged hadrons is provided in the LHCb detector by two Ring Imaging CHerenkov detectors (RICH1 and RICH2) [12, 13]. Particle identification is particularly challenging at LHCb since mass discrimination is required over the broad momentum spectrum of the particle produced. RICH detectors use the light emitted by a charged track passing through a dielectric with a velocity v greater than the speed of light in that medium, the so-called Cherenkov effect [14]. Cherenkov photons are emitted into a cone of aperture angle θ_c around the direction of propagation, with:

$$\cos(\theta_c) = \frac{c}{nv} = \frac{1}{n\beta} \tag{2.1}$$

where n is the refractive index of the medium and $\beta = v/c$. If the momentum p of a track and the associated Cherenkov angle θ_c are measured together, a determination of the mass of the charged particle (hence its type) is possible. The Cherenkov effect can happen only above a momentum threshold depending on n and the type of particle. Furthermore, for a fixed n, most of the PID sensitivity is lost at high momentum as the Cherenkov angle saturates to

$$\cos(\theta_c^{max}) \approx \frac{1}{n} \quad \text{for} \quad \beta \to 1 \tag{2.2}$$

In order to cover the momentum spectrum of the tracks produced in the collisions, LHCb uses three different radiators with different optical properties.

The RICH1 detector [15], presented in Fig. 2.15, is situated between the VELO and the dipole magnet. It is optimised to provide particle discrimination in the low

Fig. 2.15 A view of RICH1

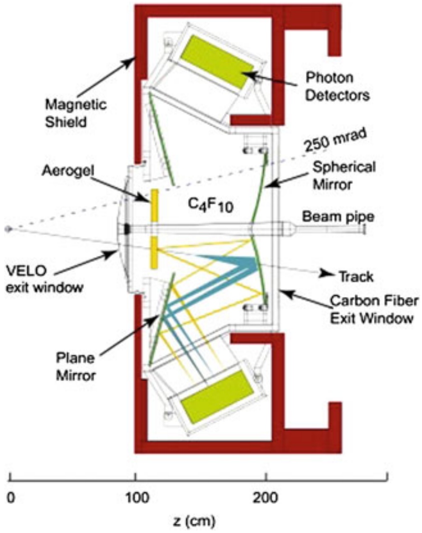

momentum range (1–60 GeV/c) with two different radiators: aerogel ($n = 1.03$) and C_4F_{10} gas ($n = 1.0014$). RICH1 covers the full LHCb angular acceptance.

The RICH2 detector [16], shown in Fig. 2.16, is located after the magnet and the tracking stations and before the calorimeters. Covering a limited angular acceptance of $\pm$ 15 to $\pm$ 200 mrad ($\pm$100mrad) in the horizontal (vertical) plane, it ensures particle identification for high momentum tracks above 15 GeV/c, up to about 100 GeV/c. The radiator used is CF_4 gas with a refractive index $n = 1.0005$.

In both RICH detectors, the Cherenkov light is deflected outside the geometrical acceptance of the detector via a set of spherical and flat mirrors and it is focused on arrays of Hybrid Photon Detectors (HPD). RICH1 (RICH2) hosts 196 (288) HPDs and each phototube is shielded from the residual magnetic field generated by the dipole.[2] HPD phototubes detect the light emitted and their information is used to reconstruct the Cherenkov cones originating from each charged track. Cones are seen as rings of hits on the phototube planes, as shown in Fig. 2.17.

2.2.6 Calorimeters

The LHCb calorimeter system [17] provides measurements of the energies and transverse positions of electrons, photons and hadrons. It plays a crucial role in the hadronic L0 trigger in order to recognise high E_T objects (Sect. 2.2.8). The classical layout of an electromagnetic calorimeter (ECAL) in front of a hadronic calorimeter

[2] Magnetic distortion corrections due to the residual magnetic field in the RICH vessels are taken into account during the offline reconstruction.

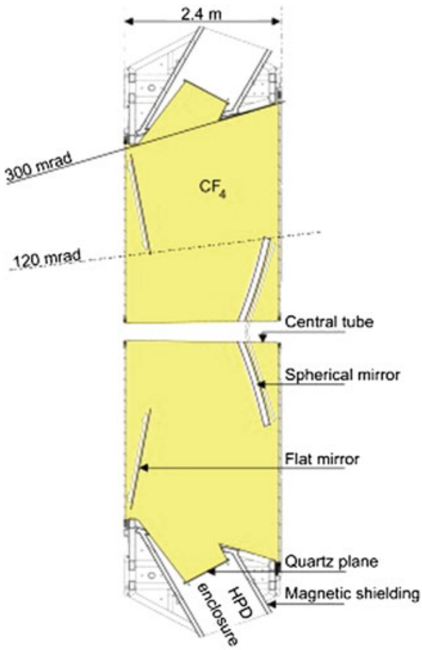

Fig. 2.16 A view of RICH2

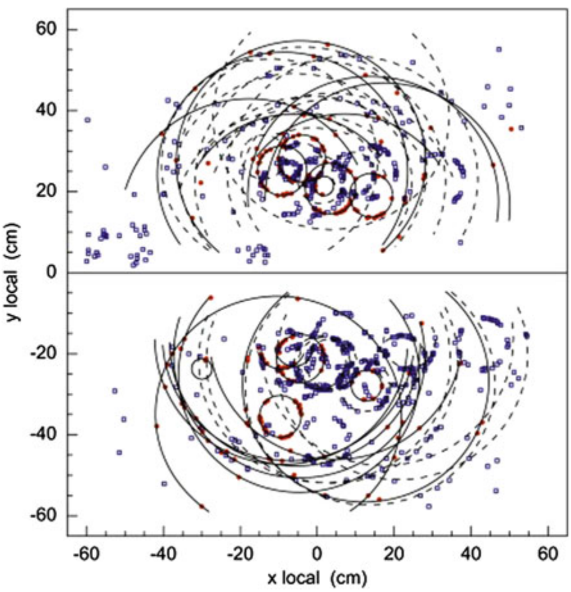

Fig. 2.17 Simulation of a LHCb event in RICH1. The Cherenkov light cones are reconstructed and fitted as rings (superimposed in the plot). The average number of Cherenkov photons emitted per track is small: about 8 in the aerogel, 30 in the C_4F_{10} and 22 in the CF_4

(HCAL) is adopted. Two additional detectors are placed in front of the ECAL to help electron discrimination from the high π^0 and γ backgrounds: the Scintillator PaD (SPD) and the Pre-Shower (PS) detectors. The calorimeters are situated between the first (M1) and the second (M2) muon stations. All calorimeter subdetectors are based on the same technology: segmented scintillators act as sensitive material and light is transported by wavelength-shifting (WLS) fibers to standard PhotoMultiplier Tubes (PMT).

SPD and PS

The Scintillator PaD (SPD) and Pre-Shower (PS) detectors are two almost identical layers of high-granularity scintillator pads. A lead converter of 15 mm, corresponding to 2.5 X_0, is located between the two scintillator planes and allows electrons to start showering before the ECAL. The SPD (PS) is situated before (after) the lead layer with a sensitive area of 7.6×6.2 m. Each scintillator tile is a square of side 3.9 cm (1,536 cells), 5.9 cm (1,792 cells) or 11.8 cm (2,688 cells) depending on the position with respect to the beamline. The geometry of a one-to-one projective correspondence with the ECAL segmentation is respected. The SPD is used to provide a good discrimination of electrons from photons in the L0 trigger and it is also used to provide a fast online estimation of the total number of charged tracks in the event. Furthermore, the background coming from charged pions is rejected analysing the longitudinal shower dispersion, measured confronting the SPD and PS hits.

ECAL

The Electromagnetic CALorimeter (ECAL) is shown in Figs. 2.18 and 2.19. It is a sampling calorimeter composed of 66 layers of lead absorber (2 mm) and scintillator

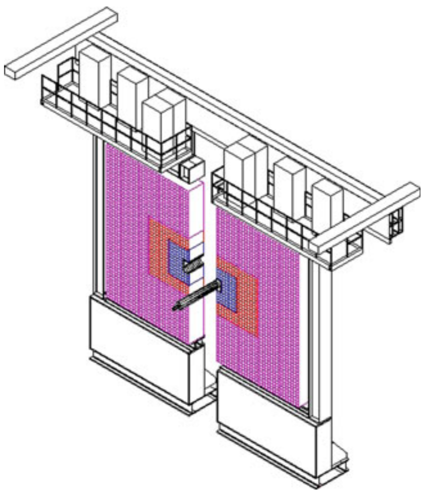

Fig. 2.18 Layout of the ECAL

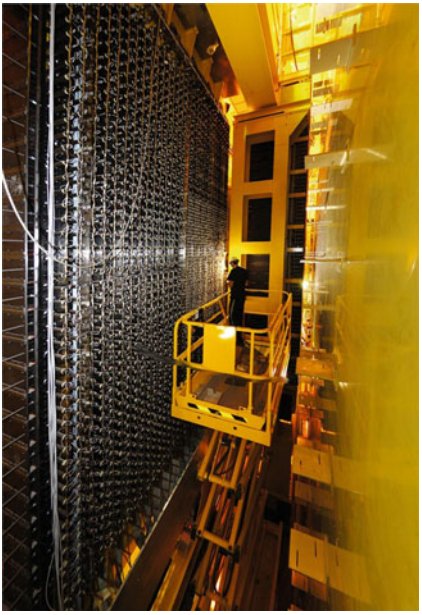

Fig. 2.19 ECAL Photomultipliers

(4 mm), corresponding to about $25\,X_0$. This ensures a good confinement of all electromagnetic-interacting particles before the HCAL. The energy resolution of the ECAL is measured to be:

$$\frac{\sigma_E}{E} = \frac{8.5 - 9.5\,\%}{\sqrt{E}} \oplus 0.8\,\% \quad \text{with } E \text{ in GeV} \tag{2.3}$$

depending on the module type, where the first term is the statistical error on the energy deposition and the second a constant term. ECAL module responses are found to be uniform within 8 % and the measured parameters are consistent with the design performance.

HCAL

The Hadronic CALorimeter (HCAL) consists of layers of iron and scintillator, with scintillator tiles orientated parallel to the z-axis. With a total dimension of 8.4 m in height, 6.8 m in width and 1.65 m in length, the detector thickness is only 5.6 λ_{int} due to space constraints in the experimental area. Therefore, hadronic showers are not fully absorbed in the calorimeter and the energy resolution is measured as:

$$\frac{\sigma_E}{E} = \frac{(69 \pm 5)\,\%}{\sqrt{E}} \oplus (9 \pm 2)\,\% \quad \text{with } E \text{ in GeV} \tag{2.4}$$

in agreement with the design values.

2.2.7 Muon Stations

The muon stations [18] are located at the end of the detector and provide efficient muon identification and triggering. The muon system is composed of five station (1,380 chambers in total) of rectangular shape: the first station M1 is located upstream the calorimeters and provides an improved p_T measurement for the trigger. The other stations (M2 to M5) are placed after the HCAL and are sandwiched with 80 cm thick iron planes. The iron absorbers stop the hadrons punching through the hadronic calorimeter and select only penetrating muons, with a minimum momentum of 6 GeV/c required to reach M5. The layout of the muon system is sketched in Fig. 2.20. The total angular acceptances are 20–306 mrad in the bending plane and 16–258 mrad in the non-bending one. Multi-Wire Proportional Chambers (MWPC) are used in all the stations, except in the inner region of M1 where triple-GEM (Gas Electron Multiplier) detectors have been preferred due to their better radiation hardness (in presence of high particle rates, GEMs can operate at higher gas gains compared to MWPCs, while decreasing the risk of discharges). The granularity of the stations is chosen according to the expected particle flux in that region. Stations M4 and M5 have limited spatial resolution and their main purpose is the identification of high p_T penetrating particles.

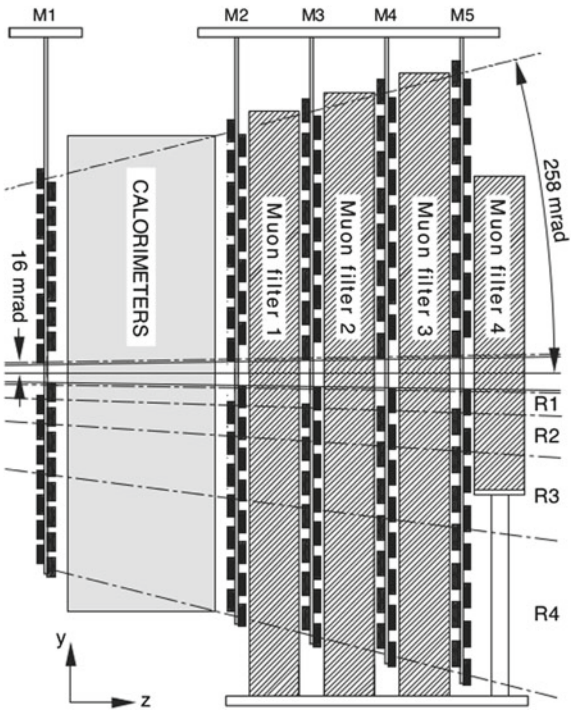

Fig. 2.20 Layout of the muon chambers and iron absorbers

2.2.8 Trigger

The LHCb detector runs a three-stage trigger [19, 20] in order to reduce the rate of visible interactions to a value of about 2–3 kHz. This represents the experimental bandwidth limit for writing events to offline storage. The LHCb trigger must be able to select the largest possible fraction of interesting collisions in a high background environment, with b and c-hadrons reconstructed into a broad range of final states. In 2010 and 2011, the LHCb experiment had to cope with running conditions very different from the design values (see Sect. 2.2.1). With visible pp collision rates of 12–15 MHz, dominated by events with multiple primary vertices, the event size has increased considerably. Therefore, the trigger working conditions had to be adjusted accordingly due to a higher-than-designed online processing time. The total output of the trigger in 2011 has been about 3 kHz, exceeding the designed value of a factor of 50 %. In 2012, the trigger output rate has been increased to 4.5 kHz.

The trigger system is divided in two levels: the Level-0 (L0) trigger and the High Level Trigger (HLT). The L0 is a hardware trigger which operates synchronously with the LHC clock, while the HLT is fully implemented within software and processes the output of the L0 on the Event Filter Farm (EFF). The EFF is composed of more than 20,000 CPU cores, which process events in parallel. The HLT is divided into two stages: the HLT1 performs only a partial inclusive reconstruction of the event and once the rate is reduced by a factor of about 20, the HLT2 performs a *almost-full* online event reconstruction and selects events for storage.

L0 Trigger

The first trigger stage, the Level-0, reduces the event rate to about 1 MHz. This is the maximum rate at which the whole detector can be read out. The L0 is a hardware trigger synchronous with the LHC clock and it is integrated in the front-end electronics of the detector. Decisions must be provided with a latency of 4 μs corresponding to the buffer time of the read-out chips. The L0 trigger exploits the large p_{T} objects produced in the event reconstructing:

- The highest E_T hadron, electron and photon clusters in the calorimeters.
- The two highest p_{T} muons in the muon stations.

These are good experimental signatures of heavy particle decays, e.g. b-hadrons, which tend to produce daughter particles with a large transverse momentum compared to the background of low-energy QCD processes. The L0 trigger is composed of three independent systems: the L0 calorimeter triggers, the L0 muon trigger and the pile-up system. Those are read in parallel and a final decision is provided by the L0 Decision Unit (L0 DU) from the logical *or* of their outputs:

- **The L0 calorimeter trigger** forms clusters of 2×2 calorimeter cells and selects those with the highest E_T. Clusters are tagged as electron (`L0Electron`), photon (`L0Photon`) or hadron (`L0Hadron`) depending on the energy deposits in the

SPD/PS, ECAL and HCAL. The HCAL is also used to reject events triggered by halo muons, while the total number of hits in the SPD is used to provide a fast, hardware estimation of the charged track multiplicity in the event.[3]

- **The L0 muon trigger** [21] looks for muon tracks with a large p_T (`L0Muon` and `L0DiMuon` lines). A fast, stand-alone procedure is used to search for hits in the muon stations compatible with a straight line pointing towards the interaction point. The highest-p_T muon segments are used for the decision.
- **The pile-up system** uses the two pile-up modules situated upstream the VELO (Sect. 2.2.2). The system was originally designed to provide a fast decision on multiple interaction events and it is currently used only to trigger beam-gas interactions.

HLT1 Trigger

The HLT1 trigger reconstructs particles in the VELO and gives a first estimation of the position of the primary vertices (PVs) in the event. HLT1 should reduce the rate to a sufficiently low level, approximately 50 kHz, to allow a complete reconstruction of the selected events in the HLT2. Several trigger decision lines are run in parallel, with a total decision time per event of order of 10–15 ms:

- **The single track trigger** [22] is used to select the decays of long-lived b and c hadrons. Its idea is to search for a single displaced high momentum track in the event. Three-dimensional VELO tracks act as a seed for reconstruction and no confirmation of the L0 trigger decision is required at this stage. A good quality track with a large impact parameter (IP) with respect to the primary vertices (PV) in the event is required to trigger the event.
- **Muon HLT1 triggers** [23] are executed only if the event has been triggered by `L0Muon` *or* `L0DiMuon` lines. All the VELO tracks are extrapolated and matched with the muon segments used in the L0 decision (there is no confirmation of the L0 candidates). This provides lifetime unbiased muon track samples. Single and di-muon lines are run depending on the requirements applied on the momentum of the particles and the invariant mass of the composed objects.
- **Electron and photon triggers** exploit the information coming from the ECAL.

HLT2 Trigger

The HLT2 trigger performs an *almost-full* pattern recognition of the events passing the HLT1 selections. Therefore, the HLT2 trigger lines use selection criteria which are as close as possible to the offline selections. The HLT2 accesses the full event information and it is able to look for secondary vertices and composed particles.

[3] In 2010, events with $n_{\text{hits}}^{\text{SPD}} > 900$ were rejected to keep the OT occupancy at about 20 %. In 2011, a looser cut of $n_{\text{hits}}^{\text{SPD}} > 600$ was chosen due to improved running conditions for the same to give better signal efficiency.

Global Event Cuts (GEC), such as the total number of reconstructed tracks, are also used to reject high multiplicity events which would require a too long processing time. A set of inclusive and exclusive selections are applied at this stage in order to take into account the largest possible number of final states.

The HLT2 muon lines are similar to those run in the HLT1, but with a more refined and complete track reconstruction. The n-body topological lines [24], instead, are designed to trigger on decays of $B \to$ anything, exploiting common decay properties of b-hadrons. In particular, $B \to DX$ decays are selected by the `Hlt2Topo2`, `Hlt2Topo3` and `Hlt2Topo4` lines, where the D meson decays into a two, three or four-body final state, respectively. Those lines are based on a fast Boosted Decision Tree (BDT) selection, which provides a good background rejection[4] and a high signal efficiency.

The HLT2-selected events are saved on permanent storage. All the created signal trigger candidates are stored in the raw event as well. This allows a direct comparison between the trigger objects that have fired a given line and the offline reconstructed signal candidates (see Sect. 3.6). In 2011, the HLT2 bandwidth was roughly shared equally among the topological, muon and charm triggers. Those lines account for almost all the total output bandwidth of about 3 kHz, as shown in Table 2.2 [25]. The rest is used by several exclusive lines, e.g. the radiative decay lines [26], and inclusive lines such as prompt J/ψ and ϕ triggers [27].

Trigger Configuration Keys (TCK)

Each trigger configuration used in data-taking is recorded and labeled via a unique identifier, called Trigger Configuration Key (TCK). Each TCK defines unambiguously the sequence of algorithms and trigger lines that have been run in the L0, HLT1

Table 2.2 Typical HLT2 trigger rates in 2011

HLT2 lines (TCK = 0x00760037, 3/8/2011)	Rate (Hz)
OR of Hlt2 *Topo decisions	1309.91
OR of Hlt2 *Charm decisions	822.92
OR of Hlt2 *SingleMuon decisions	480.91
OR of Hlt2 *DiMuon decisions	330.75
OR of Hlt2 *Muon decisions	819.34
OR of Hlt2 *DiProton decisions	45.83
OR of Hlt2 *SingleElectron decisions	1.04
OR of Hlt2 *Electron decisions	54.88
OR of Hlt2 *Gamma decisions	39.21
OR of Hlt2 *Phi decisions	77.56
OR of Hlt2 *ALL decisions	3012.19

Run: 97,871 (L0 800 kHz, $\mu = 1.4$). In the analysis presented in this thesis, all events come through the top line of the table

[4] The background rejection obtained with the BDT topological lines, used in 2011, is a factor three better than that obtained with the cut-based approach used in 2010.

and HLT2, including their configuration parameters and thresholds. TCKs are represented by a 32-bit number, with the first 16 bits reserved for the L0 configuration and the second 16 bits for the HLT. If the same lines are run, but with different thresholds, a different TCK number is associated to the new configuration. This labeling system was adopted to allow a quick configuration of the event filter farm and an easy inspection of the trigger properties.

2.2.9 Track Reconstruction

Charged tracks are refitted using the hit information coming from the VELO, TT, IT and OT [28, 29]. Depending on the properties of their trajectories, tracks can be divided into different classes, as sketched in Fig. 2.21:

- **Long tracks**
  They transverse the full tracking system, from the VELO to the last tracking station, leaving hits in all the subdetectors. These tracks have the most precisely determined momentum. All the tracks used for the analysis presented in this thesis are of this type.
- **Upstream tracks**
  They transverse only the VELO and the TT stations. These low momentum tracks are bent out of the detector acceptance by the magnetic field and they don't reach the tracking stations T1, T2 and T3. The momentum resolution on these tracks is usually poor. However, if their velocities are above the Cherenkov radiation threshold in RICH1 (Sect. 2.2.5), they can be used for its calibration.
- **Downstream tracks**
  They originate outside the VELO and they have hits only in the TT and T stations. Those highly displaced tracks are usually produced in the decay of long-lived

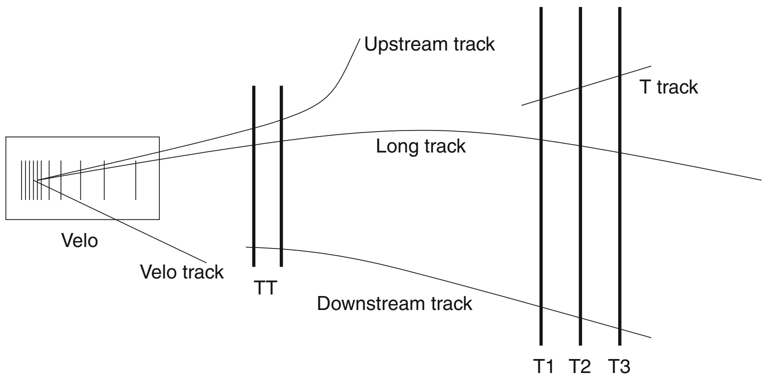

Fig. 2.21 A schematic view of the different types of charged tracks in the LHCb detector. Tracks are classified according to the detectors involved in their reconstruction

particles which decay outside the fiducial volume of the VELO, e.g. K_s^0 and Λ^0 hadrons.

- **VELO tracks**
  They exit the detector angular acceptance before the TT and have hits in the VELO detector only. Usually produced at low rapidity, they are useful for the reconstruction of the primary interaction vertices.
- **T tracks**
  They are only observed in the T stations. Produced in secondary decays, they cross the RICH2 detector and they can be used for its calibration.

An initial *seed* track is needed for the full track reconstruction. Straight-line segments of almost aligned hits are searched for in the VELO and T stations, where the magnetic field is low and a linear fit is a good approximation. After the seed tracks have been found, the hits from different detectors are matched and the trajectories refitted with a Kalman filter fit. Multiple scattering and $\mathrm{d}E/\mathrm{d}x$ energy loss are taken into account as well. The χ^2_{track} of the fit is a good indicator of the track quality and tracks with a poor χ^2_{track} can be rejected during the preliminary reconstruction of the signal candidates (see Sect. 3.4). Furthermore, a clone algorithm can check if two or more tracks have hits in common (duplicated segments) and remove any duplicated track [29].

Two important additional parameters can be introduced in order to evaluate the total performance of the track reconstruction:

- **Reconstruction efficiency**
  The reconstruction efficiency is the fraction of reconstructible tracks which are correctly reconstructed by the tracking algorithm. To be considered reconstructible, a track must lay inside the subdetectors' acceptance and give enough hits to be detected.
- **Ghost rate**
  A track is defined *ghost* if it is not matched with a charged particle in the event. These *fake* tracks are reconstructed from uncorrelated real/noise hits and have usually low momentum. The ghost rate is defined as the average fraction of ghost tracks in each event.

The reconstruction efficiency depends on several factors, e.g. the momentum spectrum of the tracks considered and the track multiplicity of the event. Using J/ψ decay products, the overall efficiency for long tracks is measured to be $95.4 \pm 0.7\,\%$ for 2010 data and $96.8 \pm 0.1\,\%$ for 2011 data [30]. The ghost rate depends on the algorithm used and it is found to be negligible for the $B \to [hh]_D h$ decays studied in this analysis.

2.2.10 Particle Identification (PID)

Particle identification of charged tracks is provided combining information coming from the RICH detectors, the calorimeters and the muon stations. For each track, all

PID contributions are merged into a log-likelihood difference ($\Delta LL_{h/\pi}$) between a given particle hypothesis h (with $h = K$, p, μ or e) and the pion hypothesis.[5] The global likelihood function is defined as:

$$\Delta LL_{h/\pi} = \ln L(h) - \ln L(\pi) = \ln \left[\frac{L(h)}{L(\pi)} \right] \tag{2.5}$$

where $L(h)$ is the likelihood of a given track of being a h hadron. It should be noted that the absolute value of the likelihood itself is not a useful quantity, as the scale changes in each event. The $\Delta LL_{h/k}$ between any h and k particle hypothesis can thus be derived trivially as follows:

$$\Delta LL_{h/k} = \Delta LL_{h/\pi} - \Delta LL_{k/\pi} = \ln L(h) - \ln L(k) = \ln \left[\frac{L(h)}{L(k)} \right] \tag{2.6}$$

The global likelihood hypothesis for each particle type is formed multiplying the different subdetector contributions:

$$L(K) = L^{\text{RICH}}(K) \cdot L^{\text{CALO}}(\text{non}\, e) \cdot L^{\text{MUON}}(\text{non}\, \mu) \tag{2.7}$$
$$L(\pi) = L^{\text{RICH}}(\pi) \cdot L^{\text{CALO}}(\text{non}\, e) \cdot L^{\text{MUON}}(\text{non}\, \mu) \tag{2.8}$$
$$L(\mu) = L^{\text{RICH}}(\mu) \cdot L^{\text{CALO}}(\text{non}\, e) \cdot L^{\text{MUON}}(\mu) \tag{2.9}$$
$$L(e) = L^{\text{RICH}}(e) \cdot L^{\text{CALO}}(e) \cdot L^{\text{MUON}}(\text{non}\, \mu) \tag{2.10}$$

Hadron Identification

Hadron discrimination derives mostly from the two RICH detectors. The circular rings observed on the phototube planes are compared with the pattern expected under a given particle hypothesis and the likelihood $L^{\text{RICH}}(h)$ is calculated from this comparison [31, 32]. The performance of particle identification is assessed on data using a series of independent, high statistics calibration modes. For example, $D^{*+} \rightarrow D^0(K^-\pi^+)\pi^+$ decays provide a large unbiased data sample of pions and kaons (for more details on the calibration procedure, see Sect. 3.11). The RICH system is designed primarily to provide an excellent K/π discrimination over a broad momentum range, as shown in Fig. 2.22 [33]. The discrimination power depends on several factors, e.g the momentum p of the particle considered.

Muon Identification

Muon identification can use information coming from the muon chambers for track with $p > 3$ GeV/c. This is the minimum momentum required to pass the

[5] The pion hypothesis is used as an arbitrary *reference* mass hypothesis.

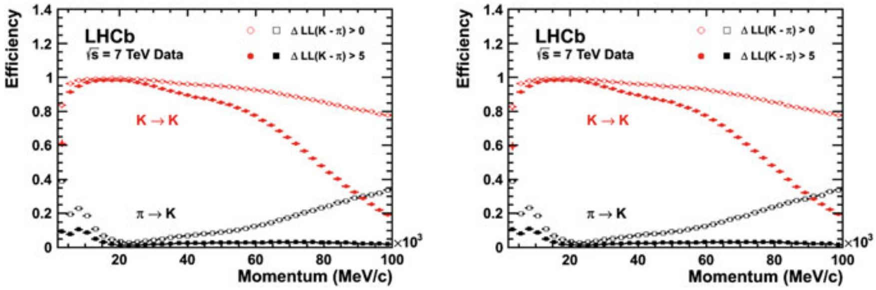

Fig. 2.22 RICH performance plots for the 2011 1.0 fb^{-1} dataset. *Left* magnet down polarity. *Right* magnet up polarity. $K \to K$ efficiency and $\pi \to K$ misidentification rate are plotted with respect to p and for two different $\Delta LL_{K/\pi}$ cuts

Table 2.3 Muon stations (from 1 to 5) required to trigger the muon decision as a function of momentum range

Momentum range	Muon stations
$3\,\text{GeV}/c < p < 6\,\text{GeV}/c$	M2 + M3
$6\,\text{GeV}/c < p < 10\,\text{GeV}/c$	M2 + M3 + (M4 or M5)
$p > 10\,\text{GeV}/c$	M2 + M3 + M4 + M5

The higher the momentum the stronger the requirement

calorimeters and reach the M2 station. Tracks are *flagged* as muons if they are associated to a certain number of hits in the five muon stations which depends on their momentum. The complete procedure is described in [34–36] and it is summarized in Table 2.3. A hit is considered consistent with a track if it is found within a Field Of Interest (FOI) defined around the track extrapolation in the muon chambers. The spatial size of the FOI is parametrized as a function of momentum and the region crossed. Furthermore, for the tracks passing the muon requirement, a hypothesis test is performed by evaluating for each track the compatibility with the muon and non-muon hypotheses. The two obtained likelihoods $L^{\text{MUON}}(\mu)$ and $L^{\text{MUON}}(\text{non }\mu)$ can be combined with the corresponding RICH likelihood $L^{\text{RICH}}(\mu)$ in order to provide a global $\Delta LL_{\mu/\pi}$ PID variable.

Electron and Neutral Particle Identification

Electron and neutral particle identification exploits the energy deposited in the ECAL to build a likelihood $L^{\text{CALO}}(h)$. As the analysis described in this thesis does not involve electrons or neutrals directly, PID at LHCb for those type of particles is not described here. More details on particle identification with the LHCb calorimeters can be found in [37], while γ and π^0 reconstruction is discussed in detail in [38].

2.2.11 LHCb Software Framework

The LHCb software environment is based upon the GAUDI framework [39]. GAUDI is a full Object Oriented framework used for all the software packages and applications of the LHCb experiment. The full Monte Carlo simulation, reconstruction and data analysis is developed in the same common environment. The main LHCb software tools are:

- GAUSS
  Simulation of LHCb events is handled by the GAUSS application [40]. GAUSS incorporates both event generation and full detector simulation tasks. *pp* primary interactions are generated with a tuned version of PYTHIA [7], while the decays of the intermediate particles are handled with the EVTGEN package [41]. After generation, the interaction of particles in the detector is described with GEANT4 [42]. Acceptance cuts can be applied at the generator level to increase the production efficiency.
- BOOLE
  The simulation of each subdetector response to the output of GAUSS is performed with a separate application: the BOOLE software package [43]. BOOLE simulates the digitization of the energy deposited in the LHCb detector active material. The L0 hardware trigger is emulated at this stage as well. The simulation of the detector electronics takes into account possible overlap between different *pp* events, the so-called spillover. The output format of BOOLE is exactly that used in real raw data files, therefore, simulated and real data files can be reconstructed with the same software chain.
- MOORE
  The Moore package [44] is used to run the HLT1 and HLT2 triggers in both the online system and offline simulated events. The trigger settings are defined via a unique Trigger Configuration Key (Sect. 2.2.8). Each TCK must be processed with a specific version of the MOORE software (the same that was run in the online event filter farm at the time data was taken) to ensure a correct reproduction of the trigger performance.
- BRUNEL
  The raw detector hits are read by BRUNEL [45] in order to reconstruct basic physics objects, e.g charged tracks, calorimeter clusters and Cherenkov rings. BRUNEL accesses the LHCb condition database in order to retrieve the experimental conditions of the detector at the time each event was taken. Physical objects are saved into .dst files for data analysis.
- DAVINCI
  DAVINCI [46] represents the last stage of the reconstruction. It is used to create composed objects, e.g. the composed particles in a decay chain, and perform cadidate selections. Several tools are available to construct and save useful quantities for offline analyses. Once candidates are selected, they can be stored in different file formats, ready for further analysis and visualization.

References

1. L. Evans, P. Bryant, LHC machine. J. Instrum. **3**(08), S08001 (2008)
2. The ATLAS Collaboration and others, The ATLAS experiment at the CERN large hadron collider. J. Instrum. **3**(08), S08003 (2008)
3. The CMS Collaboration and others, The CMS experiment at the CERN LHC. J. Instrum. **3**(08). S08004 (2008)
4. A. Alves et al., The LHCb detector at the LHC, J. Instrum. **3**, S08005 (2008) , Also published by CERN Geneva in 2010
5. The ALICE Collaboration and others, The ALICE experiment at the CERN LHC. J. Instrum. **3**(08), S08002 (2008)
6. LHCb Collaboration, R. Aaij et al., Measurement of $\sigma(pp \to b\bar{b}X)$ at $\sqrt{s} = 7$ TeV in the forward region, Phys. Lett. B**694**, 209 (2010), http://arXiv:1009.2731
7. S. Torbjörn, M. Stephen, S. Peter, PYTHIA 6.4 physics and manual, JHEP **05**, 026 (2006), arXiv:hep-ph/0603175
8. P.R. Barbosa-Marinho et al., LHCb VELO, VErtex LOcator: Technical Design Report. Technical Design Report LHCb. CERN, Geneva, 2001
9. S. Amato et al., LHCb magnet: Technical Design Report Technical Design Report LHCb. CERN, Geneva, 2000
10. P.R. Barbosa-Marinho et al., LHCb inner tracker: Technical Design Report. Technical Design Report LHCb. CERN, Geneva, 2002
11. P.R. Barbosa-Marinho et al., LHCb outer tracker: Technical Design Report. Technical Design Report LHCb. CERN, Geneva, 2001
12. S. Amato et al., LHCb RICH: Technical Design Report. Technical Design Report LHCb. CERN, Geneva, 2000
13. A. Pickford, The RICH system of the LHCb experiment: status and performance, Nucl. Instrum. Methods Phys. Res. A **604**(12), 297 (2009)
14. P.A. Cherenkov, Visible emission of clean liquids by action of γ radiation. Doklady Akademii Nauk SSSR **3**, 451 (1934)
15. N. Brook et al., LHCb RICH1 Engineering Design Review Report, Technical Report. LHCb-2004-121. CERN-LHCb-2004-121, CERN, Geneva, Oct 2005
16. E. Albrecht et al., LHCb RICH 2 engineering design review report, Technical Report. LHCb-2002-009, CERN, Geneva, May 2002
17. S. Amato et al., LHCb calorimeters: Technical Design Report. Technical Design Report LHCb. CERN, Geneva, 2000
18. P.R Barbosa-Marinho et al., LHCb muon system: Technical Design Report. Technical Design Report LHCb. CERN, Geneva, 2001
19. R. Antunes-Nobrega, et al., LHCb trigger system: Technical Design Report. Technical Design Report LHCb. CERN, Geneva, 2003. revised version number 1 submitted on 2003–09-24 12:12:22
20. H. Ruiz, The LHCb trigger: algorithms and performance, Nucl. Instrum. Methods Phys. Res., Sect. A **623**(1), 525 (2010)
21. E. Aslanides et al., The Level-0 muon trigger for the LHCb experiment, Nucl. Instrum. Methods Phys. Res., Sect. A **579**(3), 989 (2007)
22. Gligorov, V. Vladimir, A single track HLT1 trigger, Technical Report. LHCb-PUB-2011-003. CERN-LHCb-PUB-2011-003. LHCb-INT-2010-053, CERN, Geneva, Jan 2011
23. A. Roel, A. Johannes, Muon triggers in the High Level Trigger of LHCb, Tech. Rep. LHCb-PUB-2011-017. CERN-LHCb-PUB-2011-017, CERN, Geneva, Sep 2011
24. M. Williams, V. Gligorov, C. Thomas, H. Dijkstra, J. Nardulli, P. Spradlin , The HLT2 Topological Lines, Technical Report. LHCb-PUB-2011-002. CERN-LHCb-PUB-2011-002, CERN, Geneva, Jan 2011
25. https://twiki.cern.ch/twiki/bin/view/LHCb/Hlt2Rates
26. F. Soomro, V. Belyaev, HLT2 exclusive selections for $B_s \to \phi\gamma$ and $B_d \to K^*\gamma$, Technical Report. LHCb-PUB-2010-007. CERN-LHCb-PUB-2010-007, CERN, Geneva, Feb 2010

27. M. Lieng, An Inclusive phi Stream for the LHCb High Level Trigger, DC06 Analysis, Technical Report. LHCb-2009-010. CERN-LHCb-2009-010, CERN, Geneva, Jan 2009
28. O. Callot, S. Hansmann-Menzemer, The Forward Tracking: Algorithm and Performance Studies, Technical Report. LHCb-2007-015. CERN-LHCb-2007-015, CERN, Geneva, May 2007
29. https://twiki.cern.ch/twiki/bin/view/LHCb/LHCbTrackingStrategies#TrackTypes
30. A. Jaeger et al., Technical Report. LHCb-PUB-2011-025. CERN-LHCb-PUB-2011-025, CERN, Geneva, Apr 2012
31. R. Forty, RICH pattern recognition for LHCb, Nucl. Instrum. Methods Phys. Res., Sect. A **433**(12), 257 (1999)
32. M. Benayoun, C. Jones, RICH Reconstruction and Particle Identification Using Ring Fit Methods: Application to the RICH2 Detector, Technical Report. LHCb-2004-057. CERN-LHCb-2004-057, CERN, Geneva, Jan 2005
33. https://lbtwiki.cern.ch/bin/view/RICH/RichPIDPerformancePlots
34. F. Archilli et al., Muon Identification performance at LHCb with the 2010 data, Technical Report. LHCb-INT-2011-048. CERN-LHCb-INT-2011-048, CERN, Geneva, Oct 2011
35. K. Akiba, et al., Results on Muon identification efficiency with 2011 data at LHCb, Technical Report. LHCb-INT-2011-045. CERN-LHCb-INT-2011-045, CERN, Geneva, Oct 2011
36. E. Polycarpo Macedo et al., Performance of the Muon Identification in LHCb with 2011 data, Technical Report. LHCb-INT-2012-016. CERN-LHCb-INT-2012-016, CERN, Geneva, Jun 2012
37. H. Terrier, I. Belyaev, Particle identification with LHCb calorimeters, Technical Report. LHCb-2003-092, CERN, Geneva, Sep 2003
38. O. Deschamps, X. Machefert, M.H Schune, G. Pakhlova, I. Belyaev, Photon and neutral pion reconstruction, Technical Report. LHCb-2003-091, CERN, Geneva, Sep 2003
39. G. Barrand et al., GAUDI A software architecture and framework for building HEP data processing applications, Comput. Phys. Commun. **140**(12), 45 (2001)
40. I. Belyaev, P. Charpentier, S. Easo, P. Mato, J. Palacios et al., Simulation application for the LHCb experiment, eConf C0303241 (2003) TUMT003, arXiv:physics/0306035
41. D.J. Lange, The EvtGen particle decay simulation package. Nucl. Instrum. Meth. **A462**, 152 (2001)
42. GEANT4 collaboration, S. Agostinelli et al., GEANT4: A simulation toolkit, Nucl. Instrum. Meth. **A506**, 250 (2003)
43. The LHCb Collaboration, The Boole Project, http://lhcb-release-area.web.cern.ch/LHCb-release-area/DOC/boole/
44. The LHCb Collaboration, The Moore Project, http://lhcb-release-area.web.cern.ch/LHCb-release-area/DOC/moore/
45. The LHCb Collaboration, The Brunel Project, http://lhcb-release-area.web.cern.ch/LHCb-release-area/DOC/brunel/
46. The LHCb Collaboration, The DaVinci Project, http://lhcb-release-area.web.cern.ch/LHCb-release-area/DOC/davinci/

http://www.springer.com/978-3-319-01028-1

Observation of CP Violation in $B\pm \rightarrow DK\pm$ Decays
Gandini, P.
2014, XIX, 167 p. 127 illus., 115 illus. in color.,
Hardcover
ISBN: 978-3-319-01028-1